Environmental Science and Pollution Research (2022) 29:57773–57789
https://doi.org/10.1007/s11356-022-19870-z

RESEARCH ARTICLE

Removal of ammonia nitrogen, nitrate, and phosphate from aqueous solution using biochar derived from *Thalia dealbata* Fraser: effect of carbonization temperature

Yuqing Zhao[1,2] · Hang Yang[1,2] · Shibin Xia[1] · Zhenbin Wu[2]

Received: 6 January 2022 / Accepted: 19 March 2022 / Published online: 30 March 2022

Abstract

Thalia dealbata Fraser–derived biochar was prepared at different carbonization temperatures to remove nutrients in aqueous solution. Thermogravimetry/differential thermogravimetry (TG/DTG) was used to analyze the carbonization and decomposition procedure of *Thalia dealbata* Fraser. X-ray diffraction (XRD), scanning electron microscope (SEM), Fourier transform infrared spectroscopy (FTIR), zeta potential, and N_2 adsorption-desorption isotherms were employed to characterize the prepared biochar. The carbonization temperature obviously effected the physical and chemical properties of biochar. The adsorption efficiency of ammonia (NH_4^+-N), nitrate (NO_3^--N), and phosphate (PO_4^{3-}) adsorption on biochar was tested. Pseudo-first-order kinetic, pseudo-second-order kinetic, and intra-particle diffusion kinetic models were used to fit adsorption kinetic. Langmuir and Freundlich models were used to fit adsorption isotherms. The theoretical adsorption capacity of NH_4^+-N, NO_3^--N, and PO_4^{3-} on biochar was 5.8 mg/g, 3.8 mg/g, and 1.3 mg/g, respectively. This study provides the insights for effect of carbonization temperature on biochar preparation and application.

Keyword *Thalia dealbata* Fraser biochar · Carbonization temperatures · Nutrients · Adsorption

Introduction

Phosphorus and nitrogen are essential elements for the growth of organisms, and the contents of phosphorus and nitrogen in the water are the important indicators of surface water and wastewater quality (Shao et al. 2022; Wu et al. 2020). However, the presence of high concentration of phosphorus and nitrogen will reproduce the excessive algae and the eutrophication in water body, which result in the deaths of many aquatic organisms (Huang et al. 2017; Lasfar et al. 2007). At present, the methods for removing nitrogen and phosphorus mainly include coagulation technology, biological method, chemical precipitation method, ion exchange method, membrane separation method, adsorption method, etc. (Arnaldos and Pagilla 2010; Cheng et al. 2021; Guida et al. 2021; Peng et al. 2021; Qiu et al. 2020). Among them, the adsorption method has the advantages of convenient operation, low cost, and high efficiency, which is a research hotspot in the treatment of nitrogen and phosphorus wastewater (Wang et al. 2020).

Biochar is considered as a high-quality adsorption material widely used in water purification with the merit of high carbon content, developed porosity, and surface area (Liu et al. 2021; Rodríguez Alberto et al. 2021). Many studies have indicated that the biochar had certain adsorption effect for phosphorus and nitrogen in aqueous solution (Li et al. 2021a; Yang et al. 2021c). Biochar could be prepared by a wide range of raw materials, such as activated sludge, straw, and cellulose (Lawal et al. 2021; Wang et al. 2021c; Zhang et al. 2020). The physical and chemical properties of biochar are affected by many factors such as raw materials, carbonization temperature, and surface modification (Chin et al. 2021; Kasera et al. 2021; Oginni and Singh 2021). At present, the effect of raw materials and carbonization temperature for control of physical and chemical properties

Responsible Editor: Zhihong Xu

✉ Shibin Xia
xiashibin@126.com

[1] School of Resources and Environmental Engineering, Wuhan University of Technology, Wuhan 430070, China

[2] State Key Laboratory of Freshwater Ecology and Biotechnology, Institute of Hydrobiology, Chinese Academy of Sciences, Wuhan 430072, People's Republic of China

Table 1 Experimental parameters

	Initial concentration of pollutants (mg/l)	Reaction time (h)	Reaction temperature (°C)	pH
Adsorption kinetic	20	1-48	25	7
Adsorption isotherm	5–160	48	25	7
Effect of pH on adsorption	50	120	25	3–11

of prepared biochar has been extensively investigated (Cao et al. 2019; Li et al. 2021b; Yang et al. 2021b).

The wetland plants release a large amount of nitrogen and phosphorus organic substances after they are decomposed, which easily causes the siltation and blockage of the wetland substrate and affects the growth of plants (Guo et al. 2021; Yu et al. 2020). Therefore, the decomposing of wetland plants has a significant impact on the operation effect and operation life of the constructed wetland (Trevathan-Tackett et al. 2021). Plant harvesting has a significant positive impact on the reduction of nitrogen and phosphorus in water bodies. The collected plants can be made into biochar for resource utilization (Tao et al. 2019). *Thalia dealbata* Fraser is a wetland perennial emergent plant, which has a fast growth and reproduction speed (Zhang et al. 2011). Therefore, *Thalia dealbata* Fraser is an ideal material for preparation of biochar and purifying wastewater (Cui et al. 2016a). Tao et al. prepared $MgCl_2$-modified *Thalia dealbata* Fraser biochar (carbonization temperature at 500 °C) for ex situ remediation of Cd^{2+} and sulfonamide-contaminated lake sediments (Tao et al. 2019). Chu et al. studied the adsorption behavior and mechanism of anthraquinone dyes on phosphoric acid–activated *Thalia dealbata* Fraser biochar (carbonization temperature at 600 °C), with a maximum adsorption capacity of 555 mg/g (Chu et al. 2014). However, these studies mainly focus on the activation of biochar precursors and the surface modification of biochar. There are relatively few studies on the effect of carbonization temperature on biochar, which also play an important role in physical and chemical properties of biochar.

In this research, *Thalia dealbata* Fraser was used as carbon source for preparation of biochar. The chemical and physical properties of biochar prepared under different carbonization temperature were characterized using XRD, FTIR, SEM, and BET. The kinetic and isotherm behaviors of the ammonia nitrogen, nitrate, and phosphate adsorption process of biochar were investigated. The effect of pH on ammonia nitrogen, nitrate, and phosphate adsorption was studied. This paper realized the resource utilization of perennial emergent wetland plants and provided novel materials and approaches for environmental remediation.

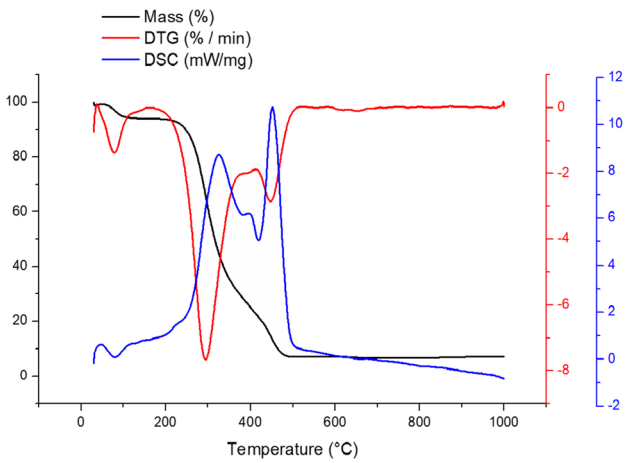

Fig. 1 The TG/DTG analysis of *Thalia dealbata* Fraser

Experimental

Materials and instruments

Preparation of *Thalia dealbata* Fraser–derived biochar *Thalia dealbata* Fraser was collected from Wuhan Optics Valley Wetland Park in autumn. The stalk of *Thalia dealbata* Fraser was cleaned, air-dried naturally (7 days), and cut into piece. The obtained stalk piece was grinded and sieved through a 100-mesh sieve, which was used as the biomass precursor for biochar preparation. Ten grams of biomass precursor was put into the crucible, and then, the crucible was put into the vacuum resistance furnace to carbonize the biomass. The parameter for carbonization was set as follows: nitrogen flow rate at 0.5 l/min, heating rate at 8 °C/min, carbonization time for 120 min, and carbonization temperature at 300°C/500°C/700°C. The obtained biochar was grinded and sieved through a 100-mesh sieve.

Table 2 The yield, pH, and CEC of biochar under different pyrolysis temperatures

Sample	Yield (%)	Ash content (%)	pH	CEC (cmol(+)/kg)
ZLH300	50.61	6.67	7.81	55.91
ZLH500	36.98	10.52	9.33	33.32
ZLH700	32.32	12.15	10.12	21.65

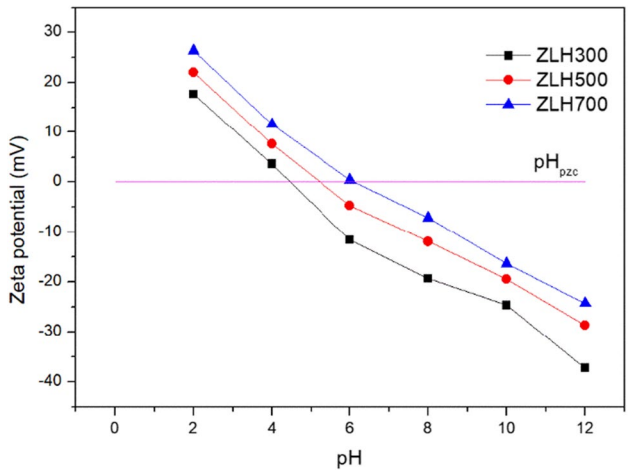

Fig. 2 The zeta potential analysis of biochar

The biochar prepared at 300°C/500°C/700°C was denoted as ZLH300, ZLH500, and ZLH700, respectively.

Materials Potassium nitrate, potassium sodium tartrate, ammonium molybdate, concentrated sulfuric acid, sulfamic acid, potassium dihydrogen phosphate, ascorbic acid, potassium persulfate, hydrochloric acid, sodium hydroxide, sodium chloride, potassium hydrogen phosphate, and sodium hydrogen carbonate were purchased from Aladdin Company. Ammonium chloride, mercury iodide, potassium iodide, and potassium dihydrogen phosphate were provided by Sinopharm Chemical Reagent Co., Ltd. All reagents used in this study was chemical analytical grade without further purification. In this experiment, all solutions were centrifuged using ultrapure water. Ammonia (NH_4^+-N), nitrate (NO_3^--N), and phosphate (PO_4^{3-}) solution were centrifuged using ammonium chloride, potassium nitrate, and potassium dihydrogen phosphate, respectively.

Instruments Field emission scanning electron microscope (FE-SEM, JSM-IT300) was employed to observe the morphology of samples. Ultraviolet-visible spectrometer (UV-Vis, QL-5800E) was used to record adsorption spectra of the solution. X-ray diffractometer (D8 Advance) was used to identify the crystal structures of the samples. A Fourier transform infrared spectrometer (FTIR, Nexus) was employed to analyze the functional groups on the samples. BET surface area analyzer (BET, ASAP 2020M) was used to determine the specific surface area and pore size of the samples. Zeta potential analyzer (NanoPlus) was used to determine the zeta potential of the samples. Comprehensive thermal analyzer (STA449F3) was used to analyze carbonization and decomposition procedure of *Thalia dealbata* Fraser. CHNS/O elemental analyzer (Vario EL cube) and inductively coupled plasma mass spectrometry (ICP-MS7400b) were used to analyze the elemental composition of the sample.

Table 4 The metal elemental content of biochar

Samples	Ca (g/kg)	Mg (g/kg)	Fe (g/kg)	Al (g/kg)
ZLH300	14.37	2.35	0.43	0.23
ZLH500	19.23	3.97	0.63	0.35
ZLH700	21.36	4.68	0.71	0.48

Analysis method of physical and chemical parameters of biochar

Yield of biochar The mass for precursor and prepared biochar was recorded. The yield of biochar was calculated according to Formula 1:

$$Y = \frac{M_1}{M} \times 100\% \quad (1)$$

In the formula, Y is the yield of biochar (%); M_1 is the mass of biochar after carbonization (g); and M is the mass of *Thalia dealbata* Fraser before burning and carbonization (g).

Ash content of biochar The ash content of biochar was determined according to standard "charcoal and charcoal test method (GB/T 17664-1999)."

CEC of biochar The cation exchange capacity (CEC) of biochar was determined according to standard "Method for measuring the exchange capacity of cation exchange resin (GB/T 8144-2008)."

pH value of biochar The pH value of biochar was determined according to standard "Wooden activated carbon test method (GB/T 12496.7-199)."

Table 3 The CNH/O elemental composition of biochar

Sample	Elements content %					Atomic ratio (%)		
	C	N	H	O	S	N/C	H/C	O + S/C
ZLH300	62.01	0.99	4.09	30.05	0.02	0.02	0.07	0.49
ZLH500	74.13	3.38	2.84	21.82	0.03	0.05	0.04	0.29
ZLH700	60.18	2.37	2.13	16.56	0.13	0.04	0.04	0.14

Table 5 BET parameters of biochar

Sample	BET surface area (m^2/g)	Micropore volume (m^3/g)	Average aperture (nm)
ZLH300	3.32	0.0036	3.35
ZLH500	13.49	0.0078	2.95
ZLH700	117.31	0.2582	1.12

Experiment section

The experimental section included the adsorption kinetics, adsorption isotherms, and effect of pH value on adsorption. In the experiment procedure, 0.1 g of biochar was put into a 200-ml Erlenmeyer flask, and then, 100 ml configured solution was put into Erlenmeyer flask. The adsorption reaction occurred by constant temperature shock box. The temperature and speed for shock box were constant at 20 °C and 180 rpm, respectively. After certain time interval, 2 ml of solution was taken out and filtered using the 0.45-μm microporous membrane. The concentration of NH_4^+-N, NO_3^--N, and PO_4^{3-} in the filtrate was measured according to standard "Nessler's reagent colorimetry (GBT 7479-87), phenol disulfonic acid spectrophotometry (GB 7480-1987), and phosphomolybdenum blue colorimetry (GBT 6913-2008)," respectively. All experiments in this study were performed for thrice. Table 1 shows the experimental parameters for adsorption.

Adsorption kinetics experiment The adsorption kinetic of pollutants on biochar included pseudo-first-order, pseudo-second-order, and intraparticle diffusivity models (Formulas 2–4) (Chaudhary et al. 2021; Ghibate et al. 2021; Sohrabi et al. 2021).

Pseudo-first-order model:

$$q_t = q_e\left(1 - e^{(-k1t)}\right) \tag{2}$$

Pseudo-second-order model:

$$\frac{t}{q_t} = \frac{1}{k_2 {q_e}^2} + \frac{t}{q_e} \tag{3}$$

Intraparticle diffusivity model:

$$Q_t = k_w t^{0.5} + b \tag{4}$$

In the formula: q_e is the adsorption capacity at equilibrium (mg/g); q_t is the adsorption capacity at t (mg/g); k_1 is the pseudo-first-order constant; k_2 is the pseudo-second-order constant; k_w and b were the intraparticle diffusivity constant, respectively.

Adsorption isotherm experiment The adsorption isotherm of pollutants on biochar included Langmuir and Freundlich models (Formulas 4–5) (Verma et al. 2021; Wang et al. 2021a).

Langmuir model:

$$\frac{C}{q_e} = \frac{C}{q_m} + \frac{1}{q_m k_1} \tag{5}$$

Freundlich model:

$$\ln q_e = \ln k_f + \frac{\ln C}{n} \tag{6}$$

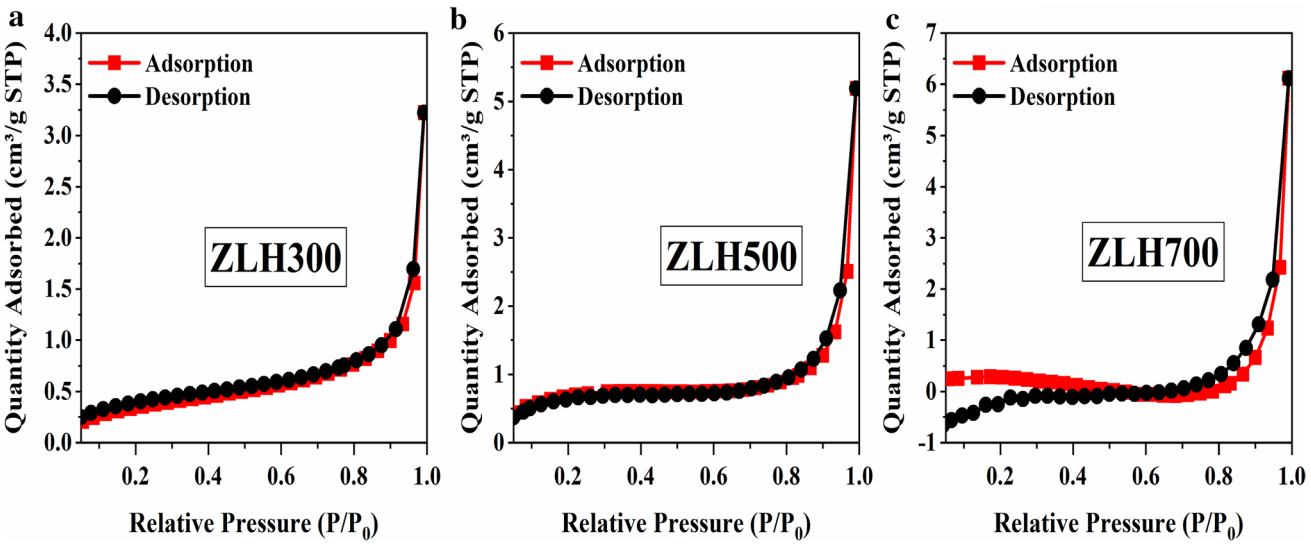

Fig. 3 The N_2 adsorption–desorption isotherms of biochar

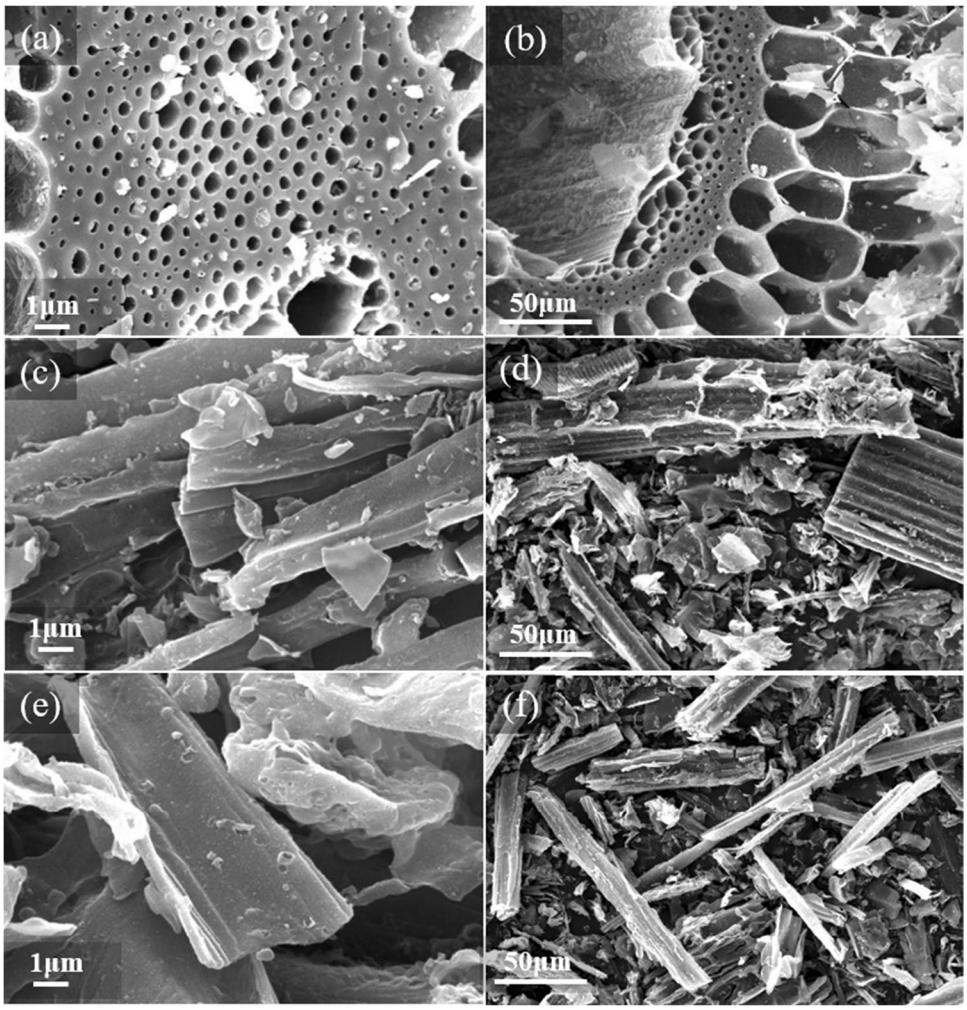

Fig. 4 The SEM scanning images of ZLH300 (**a**, **b**), ZLH500 (**c**, **d**), and ZLH700 (**e**, **f**)

In the formula: q_m is the theoretical adsorption capacity (mg/g); k_l is the Langmuir constant; k_f is the Freundlich constant.

Results and discussion

Characterization of *Thalia dealbata* Fraser and prepared biochar

Figure 1 shows the TG and DTG analysis of *Thalia dealbata* Fraser biomass. The TG curve could be divided into three stages, namely dehydration stage (25–149 °C), chain scission degradation stage (149–522 °C), and pyrolysis stage (522–1000 °C). The mass loss fraction in the dehydration stage was 5.31% which was ascribed to the evaporation of the water and free water on the surface of the biomass (Wądrzyk et al. 2021). The mass loss fraction in the degradation stage was 86.58%, which was mainly due to the evaporation of the bound water in the biomass and the decomposition of organic matter (Fan et al. 2021). This stage was the main weight loss stage of the biomass. The mass loss fraction in the pyrolysis stage was 0.98%, which was mainly due to the continued decomposition of the remaining organic matter in the biomass and the volatilization of inorganic matter. The weight of the remaining substance is less than 10% of the initial mass when the pyrolysis temperature reached 1000 °C. The value of the DSC curve was greater than > 0 under most conditions, indicating that the exothermic effect was dominated in the process of biomass pyrolysis. Two obvious peaks appear at 325.8 °C and 451.1 °C, indicating that the exothermic effect was the most obvious at this time. The value of the DTG curve was basically greater than <0, indicating that the biomass was a weightless reaction during the pyrolysis process, and a peak occurred at 294.4 °C, indicating that the high weight loss rate.

Table 2 shows the yield, ash content, pH, and CEC of biochar under different pyrolysis temperatures. As the carbonization temperature increased, the yield and CEC of biochar

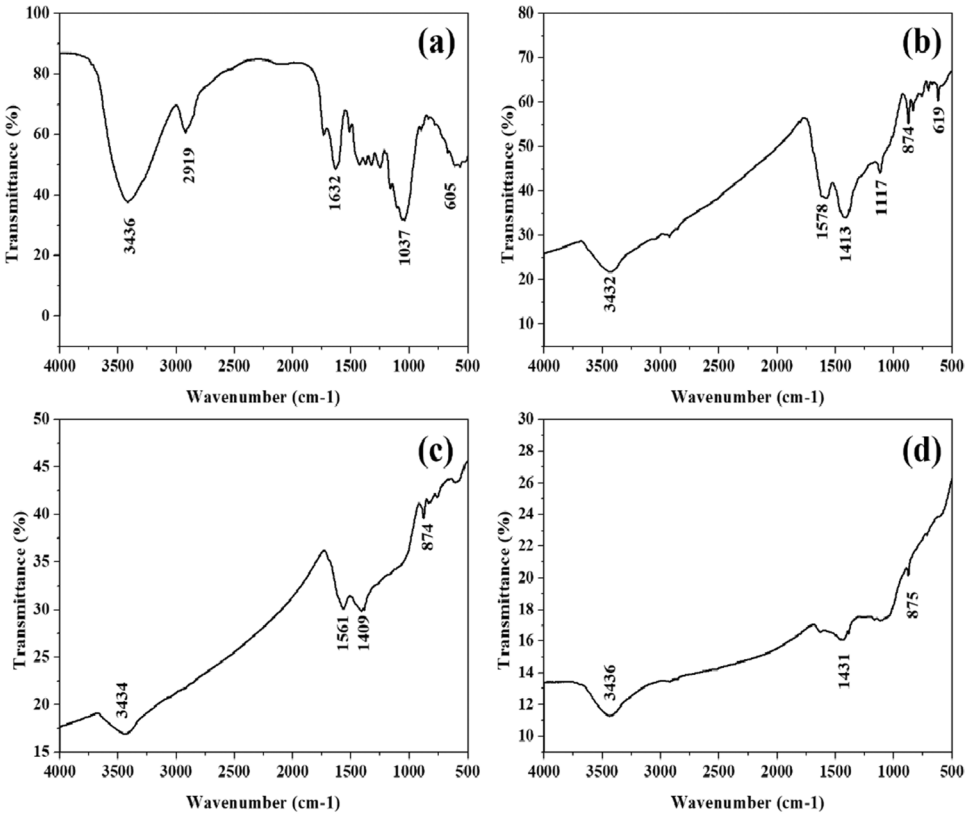

Fig. 5 FTIR spectrum of *Thalia dealbata* Fraser (**a**), ZLH300 (**b**), ZLH500 (**c**), and ZLH700 (**d**)

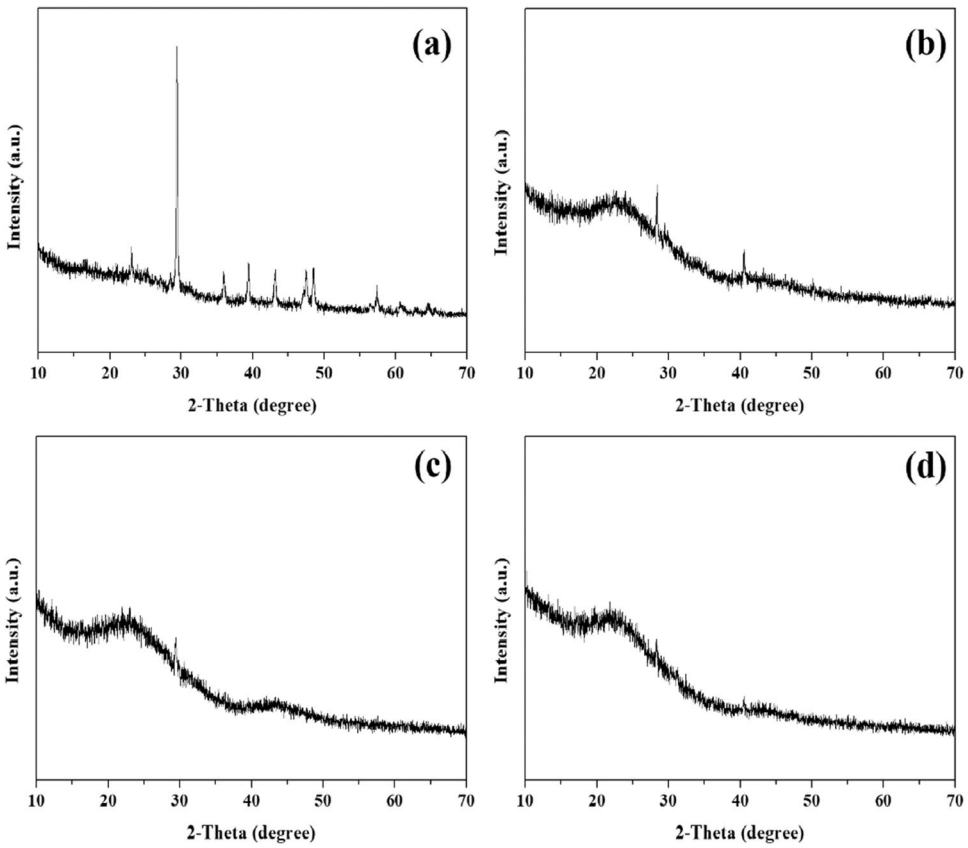

Fig. 6 The XRD patterns of *Thalia dealbata* Fraser (**a**), ZLH300 (**b**), ZLH500 (**c**), and ZLH700 (**d**)

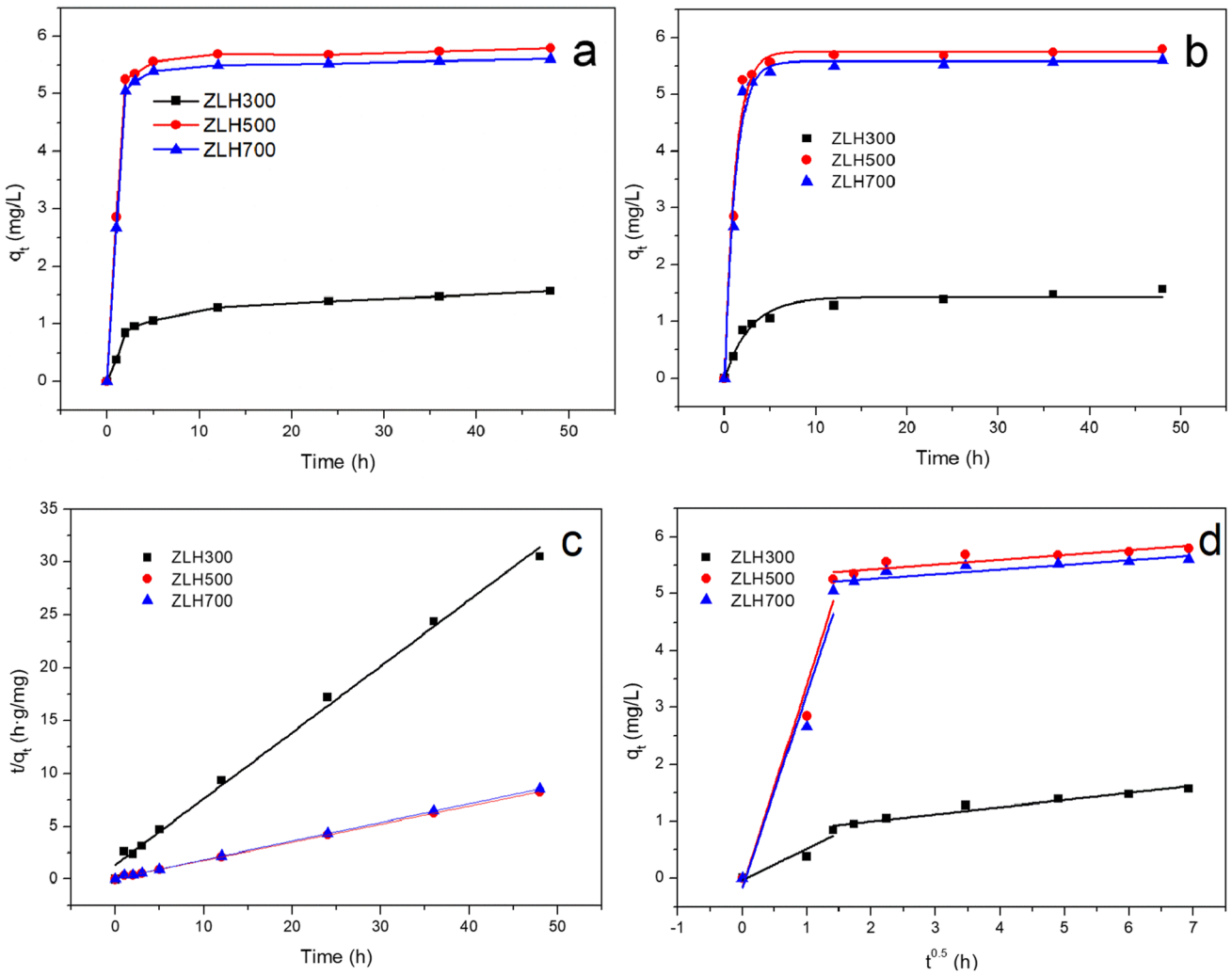

Fig. 7 Absorption kinetic of NH_4^+-N of biochar (**a**: adsorption quantity; **b**: quasi-first adsorption kinetic equation; **c**: quasi-secondary adsorption kinetic equation; **d**: intraparticle diffusivity)

decreased while ash content and pH of biochar increased. The yield of biochar decreased significantly at 300-500 °C, while the mass loss rate was relatively lower at 500–700 °C. The change in yield and ash content of biochar was ascribed to the decomposition of biomass and the relatively higher proportion of residual inorganics. With the increase of carbonization temperature, the pH value of biochar increased from 7.81 to 10.12. The alkaline dominated pH of biochar was mainly due to the fact that *Thalia dealbata* Fraser was a wetland emergent plant, which would accumulate a large amount of alkaline salt substances in the water body. As the carbonization temperature increased, the ash content in the biomass increased; meanwhile, the acidic substances (CH_4, CO_2, CO) in biomass would be volatilized. Therefore, the alkalinity of biochar gradually increased with increasing temperature. The number of functional groups on the surface of biochar was the main factor affecting the CEC of biochar (Rahman et al. 2021). Therefore, the lower CEC was imputed to the reduced oxygen-containing functional groups under higher carbonization temperature.

Figure 2 shows the zeta potential analysis of biochar by calculating the corresponding pH value when the zeta potential was 0 mV. The pH_{pzc} of ZLH300, ZLH500, and ZLH700 were calculated as 4.47, 5.24, and 6.13, respectively. When the pH value in solution was less than 4.47/5.24/6.13, the surface of ZLH300, ZLH500, and ZLH700 were positively charged; when the pH value was greater than 4.47/5.24/6.13, the surface of ZLH300, ZLH500, and ZLH700 was negatively charged. The pH_{pzc} change of biochar was positively correlated with the pH value on the biochar surface; therefore, the explanation for pH_{pzc} change was also consistent with that of the pH change on biochar.

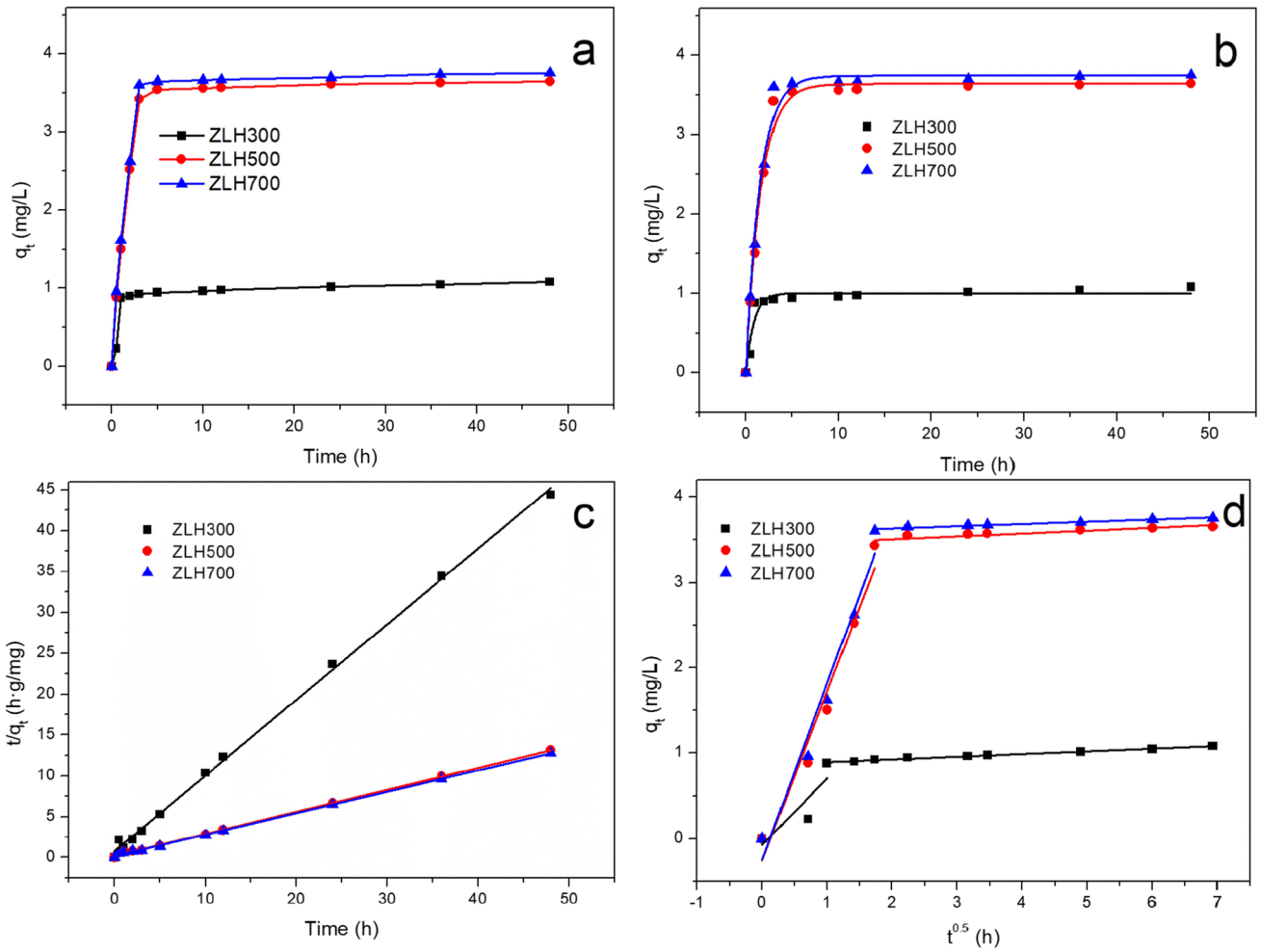

Fig. 8 Adsorption kinetic of NO_3^--N of biochar (**a**: adsorption quantity; **b**: quasi-first adsorption kinetic equation; **c**: quasi-secondary adsorption kinetic equation; **d**: intraparticle diffusivity)

Tables 3 and 4 show the CNH/O elemental composition and metal elemental content of biochar. With the increasing carbonization temperature, the element content of C and N in biochar increased and decreased consequently, while the element content of O and H gradually decreased. In addition, the ratio of H/C and O+S/C both decreased with increasing carbonization temperature, indicating that biochar has a high degree of aromaticity (Tang et al. 2021). The metal element content of biochar increased with the increase of the carbonization temperature, which was ascribed to the decomposition of organic matter in the biochar, resulting in the enhanced content of ash and inorganic salts.

Figure 3 and Table 5 show the N_2 adsorption–desorption isotherms and BET parameters of biochar, respectively. All the samples exhibited type IV isotherms with H1 hysteresis loop according to IUPAC classification (Yi et al. 2021). With increased carbonization temperature, the surface area and micropore volume of biochar increased obviously while the average aperture was reduced. The BET surface area for ZLH300, ZLH500, and ZLH700 was 3.32, 13.49, and 117.31 m^2/g, respectively. Figure 4 shows the SEM scanning images of biochar. The surface of biochar was relatively smooth and exhibited a honeycomb porous structure; when the carbonization temperature reaches 500 °C/700 °C, the structure of biochar changed significantly, and the honeycomb structure had collapsed into the form of flakes and layers.

Figure 5 shows the FTIR spectrum of samples. The surface of *Thalia dealbata* Fraser (Fig. 5a) was rich in functional groups. The characterization peak appeared at 875 cm^{-1} was ascribed to aromatic heterocyclic ring. The characterization peak appeared at 1117 cm^{-1} was imputed to C–O and C–C stretching vibration peak (Zhou et al. 2019). The characterization peaks occurred at 1440 cm^{-1} and 1400 cm^{-1} were due to $–CH_2–$ stretching vibration peak. The characterization peak occurred at 1578 cm^{-1} and 1558 cm^{-1} were owing to C=C stretching vibration peak (Li et al. 2020). The characterization peak occurred

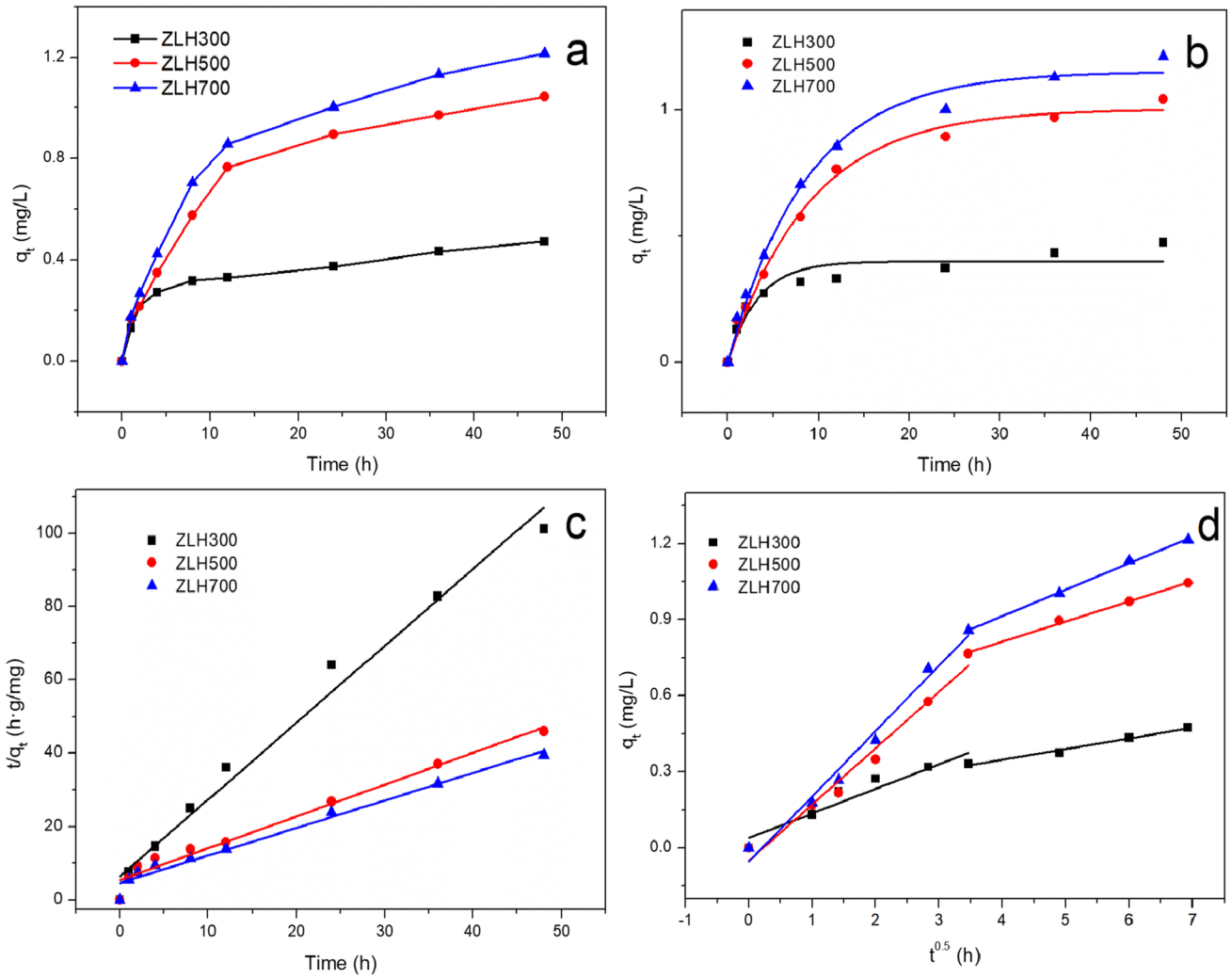

Fig. 9 The PO_4^{3-} absorption of biochar (**a**: adsorption quantity; **b**: quasi-first adsorption kinetic equation; **c**: quasi-secondary adsorption kinetic equation; **d**: intraparticle diffusivity)

at 3434 cm^{-1} was attributed to –OH stretching vibration peak (Sadhu et al. 2021). With the increase of carbonization temperature, there was no obvious shift in the position of the absorption peak, but its intensity was significantly reduced or even disappeared, indicating that high carbonization temperature would reduce the type and number of functional groups on biochar. This result was consistent with other biochars prepared from different carbon sources with different carbonization temperature (Oginni and Singh 2021; Yang et al. 2021b).

Table 6 The parameters of adsorption kinetic of NO_3^--N of different biochars

Biochar	Quasi-first-order kinetic			Quasi-secondary kinetic		
	k_1	q_e	R^2	k_2	q_e	R^2
ZLH300	0.3475	1.431	0.9622	0.2866	1.597	0.9949
ZLH500	0.8569	5.752	0.9809	0.4639	5.822	0.9996
ZLH700	0.8337	5.582	0.9790	0.4728	5.640	0.9996
Intraparticle diffusivity						
	k_w			b		R^2
ZLH300	0.5576/0.1245			−0.040/0.7522		0.8307/0.9451
ZLH500	3.554/0.0857			−0.1585/5.257		0.9327/0.7539
ZLH700	3.405/0.0826			−0.1668/5.093		0.9194/0.7273

Table 7 The parameters of adsorption kinetic of NO_3^--N on different biochars

Biochar	Quasi-first-order kinetic			Quasi-secondary kinetic		
	k_1	q_e	R^2	k_2	q_e	R^2
ZLH300	1.133	1.003	0.9151	1.131	1.080	0.9982
ZLH500	0.6214	3.644	0.9883	0.3914	3.708	0.9989
ZLH700	0.6493	3.747	0.9869	0.4049	3.810	0.9991
Intraparticle diffusivity						
	k_w			b		R^2
ZLH300	0.7766/0.0318			−0.0719/0.8597		0.5385/0.9827
ZLH500	1.976/3.432			−0.2517/3.432		0.9548/0.7514
ZLH700	2.068/0.0266			−0.2474/3.574		0.9591/0.9487

Table 8 The parameters of adsorption kinetic of PO_4^{3-} on different biochars

Biochar	Quasi-first-order kinetic			Quasi-secondary kinetic		
	k_1	q_e	R^2	k_2	q_e	R^2
ZLH300	0.3006	0.4012	0.8685	0.6813	0.4774	0.9863
ZLH500	0.1113	1.006	0.9236	0.1382	1.152	0.9944
ZLH700	0.1150	1.155	0.9820	0.1214	1.332	0.9969
Intraparticle diffusivity						
	k_w			b		R^2
ZLH300	0.8927/0.9775			0.0396/0.1799		0.8927/0.9775
ZLH500	0.9721/0.9949			−0.0499/0.4949		0.9721/0.9949
ZLH700	0.9810/0.9972			−0.0536/0.4968		0.9810/0.9972

Figure 6 shows the XRD patterns of samples. There were some diffraction peaks occurred in XRD patterns of *Thalia dealbata* Fraser (Fig. 6a), which was corresponding to the characterization peaks of cellulose and lignin (Fan et al. 2021; Wang et al. 2021b). For XRD patterns of biochar, the characteristic peaks of cellulose and lignin disappeared obviously, indicating that lignin and cellulose were destroyed during the carbonization process. In addition, an obvious bulging peak appeared at $2\theta = 23°$, indicating the amorphous phase structure of biochar (Yang et al. 2021a).

Adsorption kinetics analysis

Pseudo-first-order kinetic, pseudo-second-order kinetic, and intra-particle diffusion kinetic models were used to fit adsorption kinetic. Figures 7, 8 and 9 show the kinetic fitting curves of NH_4^+-N, NO_3^--N, and PO_4^{3-} adsorption on biochar, respectively. Tables 6, 7 and 8 show the kinetic fitting parameters. The adsorption kinetics of pollutants by the three biochars conformed to the quasi-second-order kinetic equation (most of the correlation coefficients $R^2 > 0.99$), indicating that the adsorption of pollutants by biochar was mainly controlled by the chemical adsorption mechanism.

The intra-particle diffusion model could be divided into two stages, indicating that the adsorption reaction was jointly controlled by the internal and external diffusion stages. In the initial stage of the reaction, the adsorption reaction was faster, and the fitting curve passed through the origin, indicating that the reaction stage was mainly controlled by the internal diffusion process (Islam et al. 2021). In the later stage of the reaction, the adsorption reaction speed slowed down significantly, and the fitting curve did not pass through the origin, indicating that the reaction stage was mainly controlled by the external diffusion process.

According to the parameter q_e in the quasi-secondary kinetics, the adsorption capacity of ZLH500 and ZLH700 on pollutants was relatively close, while the adsorption effect of ZLH300 on pollutants was relatively low, which was ascribed to the lower specific surface area and pore volume of ZLH300.

Adsorption isotherm analysis

Langmuir and Freundlich models were used to fit adsorption isotherms. Figures 10, 11 and 12 show the adsorption isotherms curve of NH_4^+-N, NO_3^--N, and PO_4^{3-} on biochar. Tables 9, 10 and 11 show the adsorption isotherm parameters. The correlation coefficient R^2 of Langmuir and Freundlich models was both relatively high, indicating that the two models could goodly fit the adsorption procedure. The adsorption capacity of ZLH500 and ZLH700 was relatively close, which was significantly better than those of ZLH300. According to the Langmuir model, the maximum

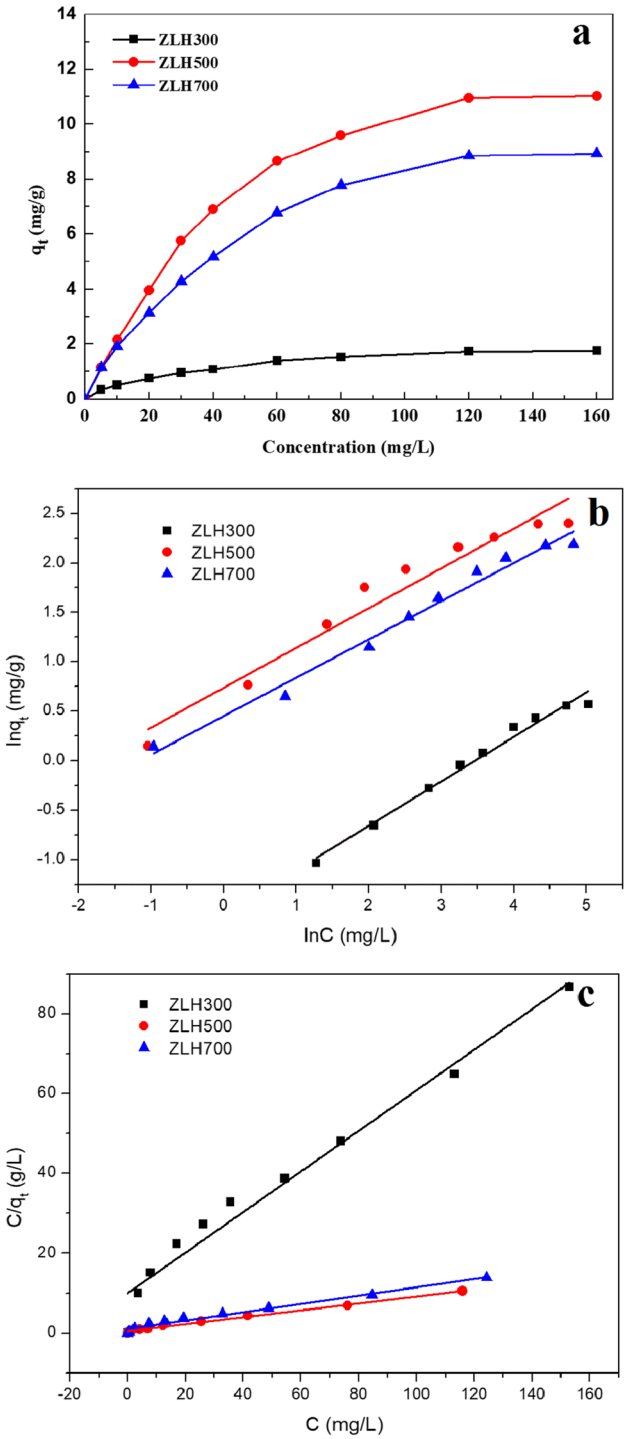

Fig. 10 Adsorption isotherm of NH_4^+-N (**a**: adsorption quantity; **b**: Freundlich; **c**: Langmuir)

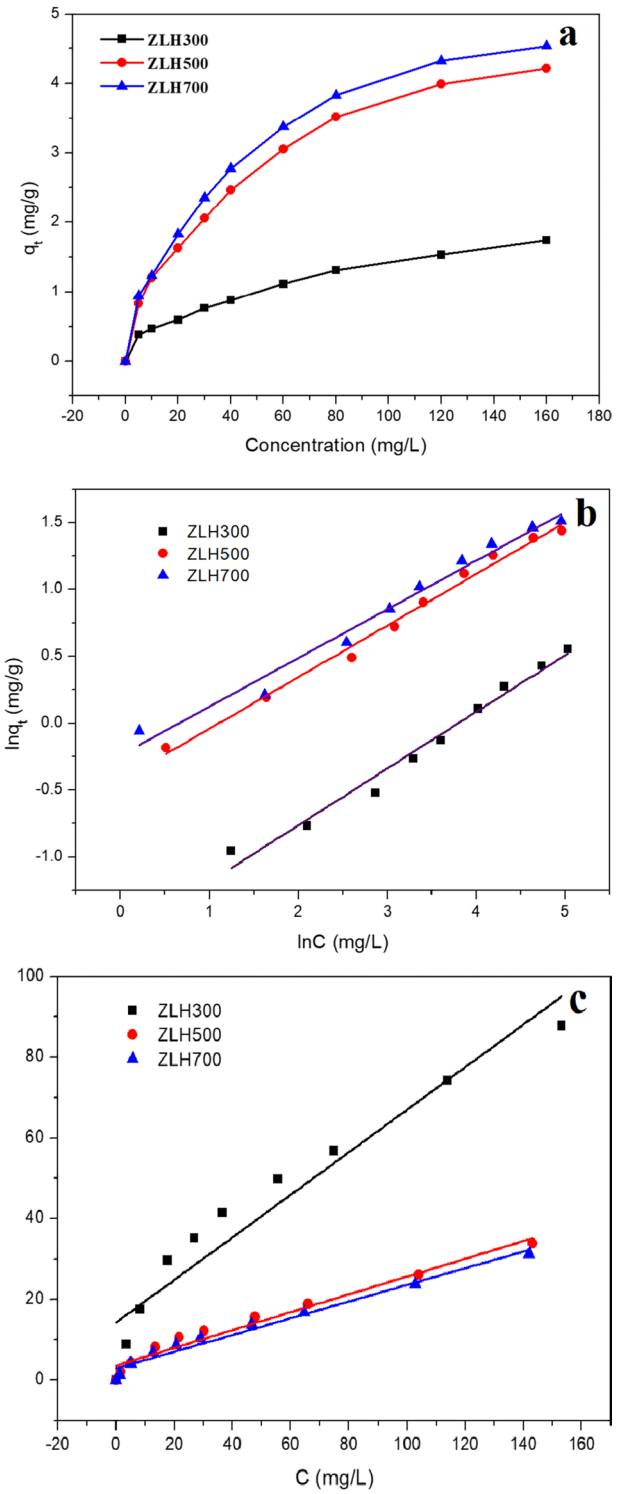

Fig. 11 Adsorption isotherm of NO_3^--N (**a**: adsorption quantity; **b**: Freundlich; **c**: Langmuir)

adsorption capacity of biochar for NH_4^+-N, NO_3^--N, and PO_4^{3-} is 15.94 mg/g (ZLH500), 5.35 mg/g (ZLH700), and 1.68 mg/g (ZLH700), respectively. According to Freundlich model calculation, all parameter values k_f were less than 1, indicating that the adsorption process was belong to preferential adsorption. At the same time, the parameter value $1/n$ was less than 1, indicating that the adsorption process was a single-layer chemical adsorption dominated behavior.

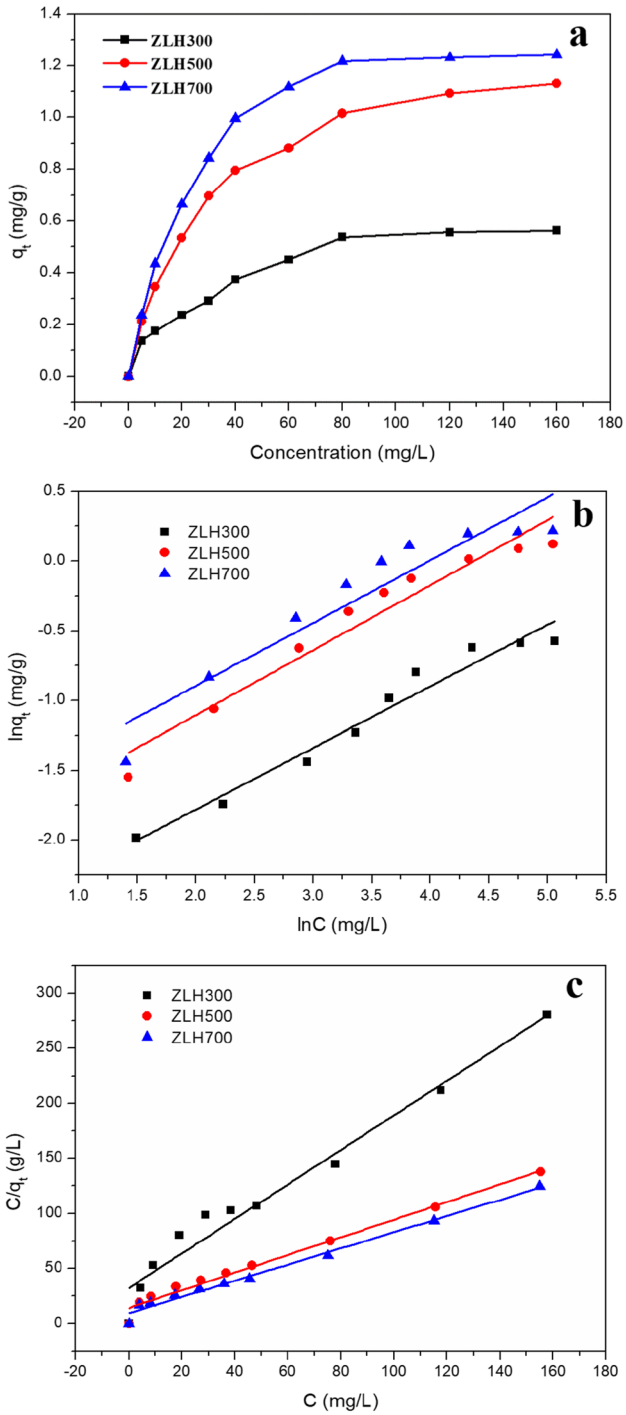

Fig. 12 Adsorption isotherm of PO_4^{3-} (**a**: adsorption quantity; **b**: Freundlich; **c**: Langmuir)

Effect of pH on adsorption of pollutant

Figure 13 shows the effect of pH on NH_4^+-N, NO_3^--N, and PO_4^{3-} adsorption on biochar. Combining the study of adsorption kinetics and adsorption isotherms, it was known that ZLH500 and ZLH700 had better adsorption effect for pollutants than that of ZLH300. Therefore, the effect of pH on the pollutant adsorption using ZLH500 and ZLH700 was studied. The optimal adsorption effect of NH_4^+-N and PO_4^{3-} was reached under neutral and weak alkaline conditions. Acidic conditions were conducive to adsorption of NO_3^--N on biochar. According to the results of the previous zeta potential analysis, the pH_{pzc} of ZLH500 and ZLH700 was 5.24 and 6.13, respectively. When the pH value of the solution was less than 5.24/6.13, the surface of ZLH500 and ZLH700 was positively charged; when the pH value was greater than 5.24/6.13, the surface of ZLH500 and ZLH700 was negatively charged. Therefore, in the adsorption process of NH_4^+-N, there was electrostatic repulsion between biochar and NH_4^+-N under acidic conditions, while under alkaline conditions, NH_4^+-N will react with OH^- to form relatively stable $NH_3{\cdot}H_2O$, which was not easy adsorbed by biochar; in the adsorption process of NO_3^--N, there was electrostatic attraction between biochar and NO_3^--N under acidic conditions while electrostatic repulsion between biochar and NO_3^--N under alkaline conditions; in the process of PO_4^{3-} adsorption, under different pH conditions, $H_2PO_4^-$ existed in different forms, relatively stable $H_2PO_4^-$ and H_3PO_4 dominated in the pH range from 2.15 to 7.20, and HPO_4^{2-} dominated in the pH range from pH 7.20 to 12.33. The free energy of adsorption of

Table 9 The parameters of adsorption isotherm of NH_4^+-N

Biochar	Langmuir			Freundlich		
	k_l	q_e	R^2	k_f	1/n	R^2
ZLH300	0.0354	2.1597	0.9645	0.4541	0.5068	0.9939
ZLH500	0.0194	15.9439	0.9576	0.7121	0.6902	0.9771
ZLH700	0.0214	12.1389	0.9725	0.6907	0.4831	0.99870

Table 10 The parameters of adsorption isotherm of NO_3^--N

Biochar	Langmuir			Freundlich		
	k_l	q_e	R^2	k_f	1/n	R^2
ZLH300	0.0960	2.0738	0.7586	0.5175	0.3905	0.9664
ZLH500	0.0781	4.9975	0.9206	0.6613	0.4916	0.9928
ZLH700	0.0564	5.3562	0.9277	0.7035	0.4783	0.9943

Table 11 The parameters of adsorption isotherm of PO_4^{3-}

Biochar	Langmuir			Freundlich		
	k_l	q_e	R^2	k_f	1/n	R^2
ZLH300	0.0406	0.6512	0.8756	0.3089	0.4602	0.9702
ZLH500	0.0363	1.3529	0.9939	0.3250	0.6311	0.9845
ZLH700	0.0346	1.6843	0.9939	0.3385	0.6631	0.9763

$H_2PO_4^-$ was lower than that of HPO_4^{2-}, resulting in the poor adsorption effect under strong acidic conditions. In addition, under strong alkali condition, there was electrostatic attraction between the biochar and HPO_4^{2-}, which also resulted in poor adsorption effect.

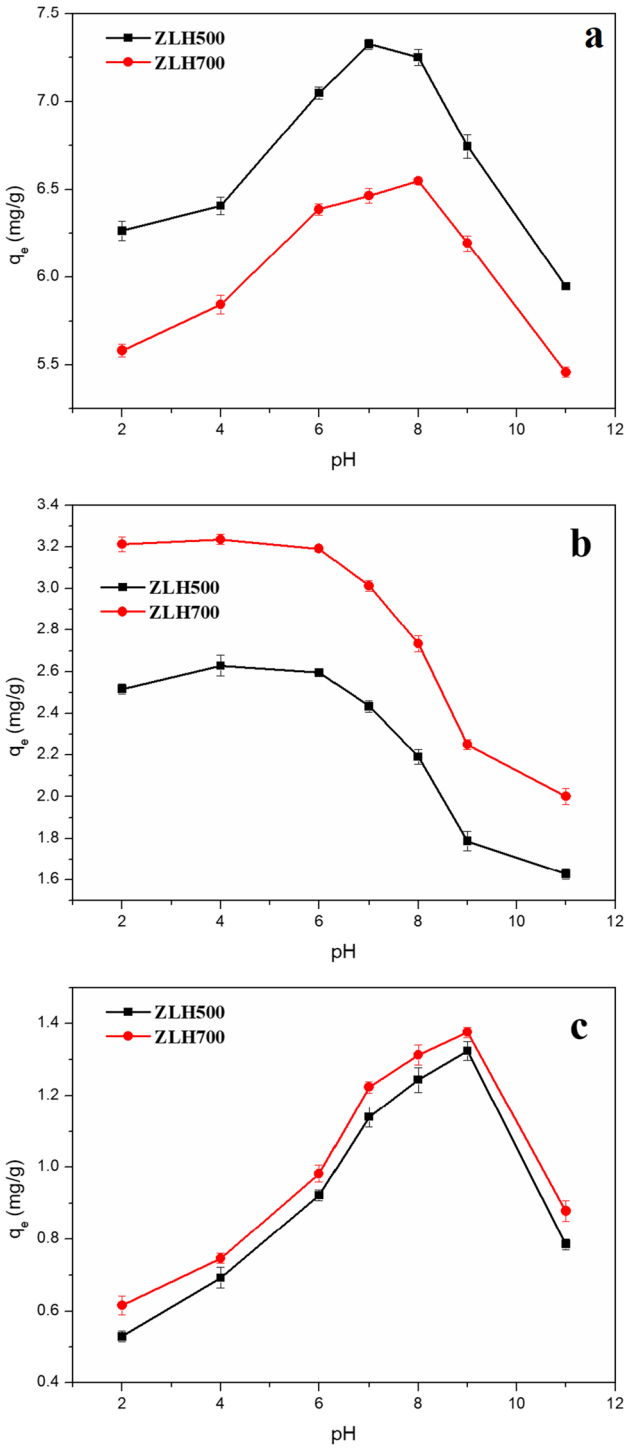

Fig. 13 The effect of pH on NH_4^+-N (**a**), NO_3^--N (**b**), and PO_4^{3-} (**c**) adsorption on biochar

Comparison with other biochar for NH_4^+-N, NO_3^--N, and PO_4^{3-} adsorptions

In order to intuitively reflect the nitrogen and phosphorus removal effect of biochar, the adsorption effect of various biochar on nitrogen and phosphorus was compared. Tables 12, 13 and 14 show the theoretical adsorption amount of nitrogen and phosphorus for biochar. In this paper, the maximum theoretical adsorption capacity of NH_4^+-N, NO_3^--N, and PO_4^{3-} was 15.9 mg/g, 5.31 mg/g and 1.6 mg/g, respectively. *Thalia dealbata* Fraser based biochar had a comparable adsorption effect on nitrogen and phosphorus with other biochars.

Discussion for possible adsorption mechanism

Generally, the adsorption behavior of biochar to inorganic pollutants can be explained from the aspects of electrostatic adsorption, ion exchange, and chemical adsorption (Chen et al. 2021; Kong et al. 2021). The electrostatic adsorption behavior was analyzed in detail in the section of pH; the electrostatic attraction behavior was possibly the main adsorption mechanism of NH_4^+-N and NO_3^--N on biochar. Ion exchange behavior can be divided into anion exchange and cation exchange. The adsorption behavior of NH_4^+-N on biochar was ascribed to the cation exchange. In the above-mentioned biochar composition, it can be found the presence of abundant Ca^{2+}, Mg^{2+}, Fe^{3+}, and Al^{3+} on the surface of biochar contains. These metal ions with strong ion exchange ability would dissociate on the surface of biochar in solution and undergone ion exchange reaction with NH^{4+}-N (Li and Shi 2022). However, the possible anion on the surface of biochar for anion exchange of NO_3^--N and PO_4^{3-} was not been identified. The chemical adsorption behavior of inorganic substances mainly involves precipitation reaction. Biochar also has the accumulation of nutrients such as nitrogen and phosphorus due to the *Thalia dealbata* Fraser is a wetland perennial emergent plant. Alkaline substance (such as Ca^{2+}/Mg^{2+}) and nitrogen and phosphorus in biochar may

Table 12 Theoretical adsorption amount of NH_4^+-N by different adsorbates

Carbon source	q_e (mg/g)	Reference
ZLH500	15.9	This study
Iron modified coconut shell biochar	0.4	Ren et al. (2021)
Activated sludge biochar	12.7	Zhang et al. (2021)
Food waste biochar	7.2	Xue et al. (2019)
Calcium Alginate Gel Beads	15.2	Yin et al. (2019)
Walnut shell composite biochar	22.9	Cheng et al. (2019)

Table 13 Theoretical adsorption amount of NO_3^--N by different dsorbates

Carbon source	q_e (mg/g)	Reference
ZLH700	5.31	This study
PAN-based activated carbon fiber	0.21	Tsuchiya et al. (2021)
Commercial Coconut Shell Biochar	1.2	Khalil et al. (2017)
Prosopis Biochar	10.9	Manjunath and Kumar (2018)
Finnish Sawdust Biochar	11.2	Kilpimaa et al. (2015)
Corn stover biochar	2.1	Tan et al. (2020)
Bamboo biochar	0.03	Yuan et al. (2021)

chemically react with NH^{4+}-N/ PO_4^{3-} to form precipitation substances such as struvite ($MgNH_4PO_3$) (Cui et al. 2016b). Therefore, the adsorption behavior of $NH4^+$-N/ PO_4^{3-} on biochar may involve chemical adsorption process.

Conclusion

In this work, *Thalia dealbata* Fraser–derived biochars were prepared at three different carbonization temperatures (300, 500, and 700 °C) and used as adsorbent for adsorption of nitrogen and phosphorus pollutants. The results indicated that with increased carbonization temperature, the yield of biochar significant decreased and the content of ash increased. In addition, the prepared biochar had higher surface area while the quantity of function group on the surface of biochar reduced obviously under higher carbonization temperature. The adsorption kinetic of pollutants on biochar conformed to the quasi-second-order and intra-particle diffusion models. Langmuir and Freundlich models both could goodly fit the adsorption isotherm procedure. ZLH500 and ZLH700 had better adsorption effect for pollutants than that of ZLH300. The maximum theoretical adsorption capacity of NH_4^+-N, NO_3^--N, and PO_4^{3-} was 15.9 mg/g, 5.31 mg/g, and 1.6 mg/g, respectively. The pH had played the important role for nitrogen and phosphorus pollutants adsorption. This study indicated the potential of resource utilization of wetland plants and illustrated the effect of carbonization temperatures on the performance of *Thalia dealbata* Fraser–derived biochar. In future studies, the practical application of *Thalia dealbata* Fraser–derived biochar in wetlands system can be investigated to achieve the virtuous circle of the ecosystem.

Table 14 Theoretical adsorption amount of phosphate by different adsorbates

Carbon source	q_e (mg/g)	Reference
ZLH700	1.6	This study
Canola straw biochar	3.1	Cao et al. (2020)
Oil palm shell biochar	0.9	Munar-Florez et al. (2021)
Mimosa biochar	5.1	Phuong Tran et al. (2021)
Orange peel biochar	1.2	Chen et al. (2011)
Sugarcane biochar	2.4	Li et al. (2016)

Acknowledgements The authors would like to thank Shiyanjia Lab (www.shiyanjia.com) for the material characterization.

Author contribution Writing — review and editing were performed by Yuqing Zhao and Hang Yang; Supervision was performed by Shibin Xia; and funding acquisition was performed by Zhenbin Wu

Funding Support was provided by the Study on Comprehensive Control of Rocky Desertification and Ecological Service Function Improvement in Karst Peaks (No. 2016YFC0502402) and Fuling Shale Gas Environmental Exploration Technology of National Science and Technology Special Project (Grant No. 2016ZX05060).

Data availability All data generated or analyzed during this study are included in this published article.

Declarations

Ethics approval and consent to participate The authors confirm that the manuscript has been read and approved by all authors. The authors declare that this manuscript has not been published and not under consideration for publication elsewhere. The authors have been personally and actively involved in substantive work leading to the manuscript and will hold themselves jointly and individually responsible for its content.

Consent for publication The authors consent to publish this research.

Competing interests The authors declare no competing interests.

References

Arnaldos M, Pagilla K (2010) Effluent dissolved organic nitrogen and dissolved phosphorus removal by enhanced coagulation and microfiltration. Water Res 44:5306–5315. https://doi.org/10.1016/j.watres.2010.06.066

Cao Y et al (2019) Impacts of carbonization temperature on the Pb(II) adsorption by wheat straw-derived biochar and related mechanism. Sci Total Environ 692:479–489. https://doi.org/10.1016/j.scitotenv.2019.07.102

Cao H, Wu X, Syed-Hassan SSA, Zhang S, Mood SH, Milan YJ, Garcia-Perez M (2020) Characteristics and mechanisms of phosphorous adsorption by rape straw-derived biochar functionalized with calcium from eggshell. Bioresour Technol 318:124063. https://doi.org/10.1016/j.biortech.2020.124063

Chaudhary M, Jain N, Maiti A (2021) A comparative adsorption kinetic modeling of fluoride adsorption by nanoparticles and its polymeric nanocomposite Journal of Environmental. Chem Eng 9:105595. https://doi.org/10.1016/j.jece.2021.105595

Chen B, Chen Z, Lv S (2011) A novel magnetic biochar efficiently sorbs organic pollutants and phosphate. Bioresour Technol 102:716–723. https://doi.org/10.1016/j.biortech.2010.08.067

Chen M, Wang F, Zhang D-l, Yi W-m, Liu Y (2021) Effects of acid modification on the structure and adsorption NH4+-N properties of biochar. Renewable Energy 169:1343–1350. https://doi.org/10.1016/j.renene.2021.01.098

Cheng H, Zhu Q, Xing Z (2019) Adsorption of ammonia nitrogen in low temperature domestic wastewater by modification bentonite. J Cleaner Prod 233:720–730. https://doi.org/10.1016/j.jclepro.2019.06.079

Cheng N, Wang B, Feng Q, Zhang X, Chen M (2021) Co-adsorption performance and mechanism of nitrogen and phosphorus onto eupatorium adenophorum biochar in water. Bioresour Technol 340:125696. https://doi.org/10.1016/j.biortech.2021.125696

Chin JF, Heng ZW, Teoh HC, Chan Chong W, Pang YL (2021) A review on recent development of magnetic biochar crosslinked chitosan on heavy metal removal from wastewater – modification, application and mechanism Chemosphere:133035 doi:https://doi.org/10.1016/j.chemosphere.2021.133035

Chu SY, Xiao JB, Tian GM, Wong MH (2014) Preparation and characterization of activated carbon from aquatic macrophyte debris and its ability to adsorb anthraquinone dyes. J Indust Eng Chem 20:3461–3466. https://doi.org/10.1016/j.jiec.2013.12.035

Cui X, Dai X, Khan KY, Li T, Yang X, He Z (2016a) Removal of phosphate from aqueous solution using magnesium-alginate/chitosan modified biochar microspheres derived from Thalia dealbata. Bioresour Technol 218:1123–1132. https://doi.org/10.1016/j.biortech.2016.07.072

Cui X, Hao H, Zhang C, He Z, Yang X (2016b) Capacity and mechanisms of ammonium and cadmium sorption on different wetland-plant derived biochars. Sci Total Environ 539:566–575. https://doi.org/10.1016/j.scitotenv.2015.09.022

Fan M, Li C, Sun Y, Zhang L, Zhang S, Hu X (2021) In situ characterization of functional groups of biochar in pyrolysis of cellulose. Sci Total Environ 799:149354. https://doi.org/10.1016/j.scitotenv.2021.149354

Ghibate R, Senhaji O, Taouil R (2021) Kinetic and thermodynamic approaches on Rhodamine B adsorption onto pomegranate peel Case Studies in Chemical and Environmental. Engineering 3:100078. https://doi.org/10.1016/j.cscee.2020.100078

Guida S, Rubertelli G, Jefferson B, Soares A (2021) Demonstration of ion exchange technology for phosphorus removal and recovery from municipal wastewater. Chem Eng J 420:129913. https://doi.org/10.1016/j.cej.2021.129913

Guo Y, Boughton EH, Qiu J (2021) Interactive effects of land-use intensity, grazing and fire on decomposition of subtropical seasonal wetlands Ecol Indicators 132:108301. https://doi.org/10.1016/j.ecolind.2021.108301

Huang J, Xu C-c, Ridoutt BG, Wang X-c, Ren P-a (2017) Nitrogen and phosphorus losses and eutrophication potential associated with fertilizer application to cropland in China. J Cleaner Prod 159:171–179. https://doi.org/10.1016/j.jclepro.2017.05.008

Islam MS et al (2021) Biochar heavy metal removal in aqueous solution depends on feedstock type and pyrolysis purging gas. Environ Pollut 281:117094. https://doi.org/10.1016/j.envpol.2021.117094

Kasera N, Hall S, Kolar P (2021) Effect of surface modification by nitrogen-containing chemicals on morphology and surface characteristics of N-doped pine bark biochars Journal of Environmental. Chem Eng 9:105161. https://doi.org/10.1016/j.jece.2021.105161

Khalil AME, Eljamal O, Amen TWM, Sugihara Y, Matsunaga N (2017) Optimized nano-scale zero-valent iron supported on treated activated carbon for enhanced nitrate and phosphate removal from water. Chem Eng J 309:349–365. https://doi.org/10.1016/j.cej.2016.10.080

Kilpimaa S, Runtti H, Kangas T, Lassi U, Kuokkanen T (2015) Physical activation of carbon residue from biomass gasification: novel sorbent for the removal of phosphates and nitrates from aqueous solution. J Indust Eng Chem 21:1354–1364. https://doi.org/10.1016/j.jiec.2014.06.006

Kong W, Zhang M, Liu Y, Gou J, Wei Q, Shen B (2021) Physicochemical characteristics and the adsorption of ammonium of biochar pyrolyzed from distilled spirit lees, tobacco fine and Chinese medicine residues. J Anal Appl Pyrolysis 156:105148. https://doi.org/10.1016/j.jaap.2021.105148

Lasfar S, Monette F, Millette L, Azzouz A (2007) Intrinsic growth rate: a new approach to evaluate the effects of temperature, photoperiod and phosphorus–nitrogen concentrations on duckweed growth under controlled eutrophication. Water Res 41:2333–2340. https://doi.org/10.1016/j.watres.2007.01.059

Lawal AA, Hassan MA, Zakaria MR, Yusoff MZM, Norrrahim MNF, Mokhtar MN, Shirai Y (2021) Effect of oil palm biomass cellulosic content on nanopore structure and adsorption capacity of biochar. Bioresour Technol 332:125070. https://doi.org/10.1016/j.biortech.2021.125070

Li X, Shi J (2022) Simultaneous adsorption of tetracycline, ammonium and phosphate from wastewater by iron and nitrogen modified biochar: kinetics, isotherm, thermodynamic and mechanism. Chemosphere 293:133574. https://doi.org/10.1016/j.chemosphere.2022.133574

Li R et al (2016) Recovery of phosphate from aqueous solution by magnesium oxide decorated magnetic biochar and its potential as phosphate-based fertilizer substitute. Bioresour Technol 215:209–214. https://doi.org/10.1016/j.biortech.2016.02.125

Li R, Huang J, Li J, Cao L, Zhong X, Yu A, Lu G (2020) Nitrogen-doped porous hard carbons derived from shaddock peel for high-capacity lithium-ion battery anodes. J Electroanal Chem 862:114044. https://doi.org/10.1016/j.jelechem.2020.114044

Li B, Jing F, Hu Z, Liu Y, Xiao B, Guo D (2021a) Simultaneous recovery of nitrogen and phosphorus from biogas slurry by Fe-modified biochar. J Saudi Chem Soc 25:101213. https://doi.org/10.1016/j.jscs.2021.101213

Li B, Zhang Y, Xu J, Mei Y, Fan S, Xu H (2021b) Effect of carbonization methods on the properties of tea waste biochars and their application in tetracycline removal from aqueous solutions. Chemosphere 267:129283. https://doi.org/10.1016/j.chemosphere.2020.129283

Liu T, Lawluvy Y, Shi Y, Ighalo JO, He Y, Zhang Y, Yap P-S (2021) Adsorption of cadmium and lead from aqueous solution using modified biochar: a review. J Environ Chem Eng:106502. https://doi.org/10.1016/j.jece.2021.106502

Manjunath SV, Kumar M (2018) Evaluation of single-component and multi-component adsorption of metronidazole, phosphate and nitrate on activated carbon from Prosopıs julıflora. Chem Eng J 346:525–534. https://doi.org/10.1016/j.cej.2018.04.013

Munar-Florez DA, Varón-Cardenas DA, Ramírez-Contreras NE, García-Núñez JA (2021) Adsorption of ammonium and phosphates by biochar produced from oil palm shells: effects of production conditions. Results Chem 3:100119. https://doi.org/10.1016/j.rechem.2021.100119

Oginni O, Singh K (2021) Effect of carbonization temperature on fuel and caffeine adsorption characteristics of white pine and Norway spruce needle derived biochars. Industrial Crops Products 162:113261. https://doi.org/10.1016/j.indcrop.2021.113261

Peng Y, He S, Wu F (2021) Biochemical processes mediated by iron-based materials in water treatement: enhancing nitrogen and phosphorus removal in low C/N ratio wastewater. Sci Total

Environ 775:145137. https://doi.org/10.1016/j.scitotenv.2021.145137

Phuong Tran TC, Nguyen TP, Nguyen Nguyen TT, Thao Tran TN, Hang Nguyen TA, Tran QB, Nguyen XC (2021) Enhancement of phosphate adsorption by chemically modified biochars derived from Mimosa pigra invasive plant Case Studies in Chemical and Environmental. Engineering 4:100117. https://doi.org/10.1016/j.cscee.2021.100117

Qiu B et al (2020) Simultaneous recovery of phosphorus and nitrogen from liquid digestate by vacuum membrane distillation with permeate fractional condensation. Chin J Chem Eng 28:1558–1565. https://doi.org/10.1016/j.cjche.2020.01.019

Rahman MYA, Cooper R, Truong N, Ergas SJ, Nachabe MH (2021) Water quality and hydraulic performance of biochar amended biofilters for management of agricultural runoff. Chemosphere 283:130978. https://doi.org/10.1016/j.chemosphere.2021.130978

Ren Z, Jia B, Zhang G, Fu X, Wang Z, Wang P, Lv L (2021) Study on adsorption of ammonia nitrogen by iron-loaded activated carbon from low temperature wastewater. Chemosphere 262:127895. https://doi.org/10.1016/j.chemosphere.2020.127895

Rodríguez Alberto D, Tyler AC, Trabold TA (2021) Phosphate adsorption using biochar derived from solid digestate. Bioresource Technol Reports 16:100864. https://doi.org/10.1016/j.biteb.2021.100864

Sadhu M, Bhattacharya P, Vithanage M, Padmaja Sudhakar P (2021) Adsorptive removal of fluoride using biochar – a potential application in drinking water treatment. Sep Purif Technol 278:119106. https://doi.org/10.1016/j.seppur.2021.119106

Shao Q et al (2022) Phosphorus and nitrogen recovery from wastewater by ceramsite: adsorption mechanism, plant cultivation and sustainability analysis. Sci Total Environ 805:150288. https://doi.org/10.1016/j.scitotenv.2021.150288

Sohrabi N, Mohammadi R, Ghassemzadeh HR, Heris SSS (2021) Equilibrium, kinetic and thermodynamic study of diazinon adsorption from water by clay/GO/Fe3O4: modeling and optimization based on response surface methodology and artificial neural network. J Mol Liq 328:115384. https://doi.org/10.1016/j.molliq.2021.115384

Tan G, Mao Y, Wang H, Xu N (2020) A comparative study of arsenic(V), tetracycline and nitrate ions adsorption onto magnetic biochars and activated carbon. Chem Eng Res Des 159:582–591. https://doi.org/10.1016/j.cherd.2020.05.011

Tang W, Zanli BLGL, Chen J (2021) O/N/P-doped biochar induced to enhance adsorption of sulfonamide with coexisting Cu2+/Cr (VI) by air pre-oxidation. Bioresour Technol 341:125794. https://doi.org/10.1016/j.biortech.2021.125794

Tao Q et al (2019) Simultaneous remediation of sediments contaminated with sulfamethoxazole and cadmium using magnesium-modified biochar derived from Thalia dealbata. Sci Total Environ 659:1448–1456. https://doi.org/10.1016/j.scitotenv.2018.12.361

Trevathan-Tackett SM et al (2021) Ecosystem type drives tea litter decomposition and associated prokaryotic microbiome communities in freshwater and coastal wetlands at a continental scale. Sci Total Environ 782:146819. https://doi.org/10.1016/j.scitotenv.2021.146819

Tsuchiya Y, Yamaya Y, Amano Y, Machida M (2021) Effect of two types of adsorption sites of activated carbon fibers on nitrate ion adsorption. J Environ Manage 289:112484. https://doi.org/10.1016/j.jenvman.2021.112484

Verma M, Tyagi I, Kumar V, Goel S, Vaya D, Kim H (2021) Fabrication of GO-MnO2 nanocomposite using hydrothermal process for cationic and anionic dyes adsorption: kinetics, isotherm, and reusability. J Environ Chem Eng:106045. https://doi.org/10.1016/j.jece.2021.106045

Wądrzyk M, Grzywacz P, Janus R, Michalik M (2021) A two-stage processing of cherry pomace via hydrothermal treatment followed by biochar gasification. Renewable Energy 179:248–261. https://doi.org/10.1016/j.renene.2021.06.130

Wang Y, Yang X, Jing X, Dai J, Dong M, Yan Y (2020) Adsorption of phosphorus on lanthanum doped carbon films guided by self-assembly of cellulose nanocrystalline. J Mol Liq 319:114148. https://doi.org/10.1016/j.molliq.2020.114148

Wang R, Liu H, Dou L, Bai H, Zhang N (2021a) Effect of adsorption phase and matrix deformation on methane adsorption isotherm of Fuling shale. J Natural Gas Sci Eng:104018. https://doi.org/10.1016/j.jngse.2021.104018

Wang W, Liu Y, Wang Y, Liu L, Hu C (2021b) Effect of nickel salts on the production of biochar derived from alkali lignin: properties and applications. Bioresour Technol 341:125876. https://doi.org/10.1016/j.biortech.2021.125876

Wang Z, Xu J, Yellezuome D, Liu R (2021c) Effects of cotton straw-derived biochar under different pyrolysis conditions on Pb (II) adsorption properties in aqueous solutions. J Anal Appl Pyrolysis 157:105214. https://doi.org/10.1016/j.jaap.2021.105214

Wu L, Zhang S, Wang J, Ding X (2020) Phosphorus retention using iron (II/III) modified biochar in saline-alkaline soils: adsorption, column and field tests. Environ Pollut 261:114223. https://doi.org/10.1016/j.envpol.2020.114223

Xue S et al (2019) Food waste based biochars for ammonia nitrogen removal from aqueous solutions. Bioresour Technol 292:121927. https://doi.org/10.1016/j.biortech.2019.121927

Yang H, Sun J, Zhang Y, Xue Q, Xia S (2021a) Preparation of hydrophobic carbon aerogel using cellulose extracted from luffa sponge for adsorption of diesel oil. Ceram Int. https://doi.org/10.1016/j.ceramint.2021.08.294

Yang Z, Hou J, Wu J, Miao L (2021b) The effect of carbonization temperature on the capacity and mechanisms of Pb(II) adsorption by microalgae residue-derived biochar. Ecotoxicol Environ Saf 225:112750. https://doi.org/10.1016/j.ecoenv.2021.112750

Yang Z et al (2021c) Tuning adsorption capacity of metal–organic frameworks with Al3+ for phosphorus removal: kinetics, isotherm and regeneration Inorg. Chem Commun 132:108804. https://doi.org/10.1016/j.inoche.2021.108804

Yi Y, Tu G, Ying G, Fang Z, Tsang EP (2021) Magnetic biochar derived from rice straw and stainless steel pickling waste liquor for highly efficient adsorption of crystal violet. Bioresour Technol 341:125743. https://doi.org/10.1016/j.biortech.2021.125743

Yin Q, Liu M, Ren H (2019) Biochar produced from the co-pyrolysis of sewage sludge and walnut shell for ammonium and phosphate adsorption from water. J Environ Manage 249:109410. https://doi.org/10.1016/j.jenvman.2019.109410

Yu X, Ding S, Lin Q, Wang G, Wang C, Zheng S, Zou Y (2020) Wetland plant litter decomposition occurring during the freeze season under disparate flooded conditions. Sci Total Environ 706:136091. https://doi.org/10.1016/j.scitotenv.2019.136091

Yuan J, Amano Y, Machida M (2021) Surface characterization of mesoporous biomass activated carbon modified by thermal chemical vapor deposition and adsorptive mechanism of nitrate ions in aqueous solution. Colloids Surf Physicochem Eng Aspects 616:126213. https://doi.org/10.1016/j.colsurfa.2021.126213

Zhang T-t, Wang L-l, He Z-x, Zhang D (2011) Growth inhibition and biochemical changes of cyanobacteria induced by emergent macrophyte Thalia dealbata roots. Biochem Syst Ecol 39:88–94. https://doi.org/10.1016/j.bse.2011.01.004

Zhang J et al (2020) Effect of deashing on activation process and lead adsorption capacities of sludge-based biochar. Sci Total Environ 716:137016. https://doi.org/10.1016/j.scitotenv.2020.137016

Zhang L, Deng F, Liu Z, Ai L (2021) Removal of ammonia nitrogen and phosphorus by biochar prepared from sludge residue after

rusty scrap iron and reduced iron powder enhanced fermentation. J Environ Manage 282:111970. https://doi.org/10.1016/j.jenvman.2021.111970

Zhou Y, Cao S, Xi C, Li X, Zhang L, Wang G, Chen Z (2019) A novel Fe3O4/graphene oxide/citrus peel-derived bio-char based nanocomposite with enhanced adsorption affinity and sensitivity of ciprofloxacin and sparfloxacin. Bioresour Technol 292:121951. https://doi.org/10.1016/j.biortech.2019.121951